

NASA Contractor Report 3344

TECH LIBRARY KAFB, NM



0094646

**Electrostatic Protection of the  
Solar Power Satellite and Rectenna**  
Part I: Protection of the Solar Power Satellite

*Rice University  
Houston, Texas*

Prepared for  
Marshall Space Flight Center  
under Contract NAS8-33023

**NASA**

National Aeronautics  
and Space Administration

**Scientific and Technical  
Information Branch**

1980

## Introduction

Space is by no means empty. It contains light, magnetic fields and both neutral and charged particles. The light energy is the *raison d'être* for space power generation; but it can also eject photoelectrons from satellite surfaces, giving the surface a positive charge and giving it an effective conductivity (Pelizzari and Criswell, 1978).

Magnetic field strengths in the earth's vicinity range from  $6 \times 10^{-5} \text{ T}$  (0.6 Gauss) at the earth's poles to  $2 \times 10^{-9} \text{ T}$  ( $2\gamma$ ) in the neutral sheet in the magnetotail ( $1\gamma = 10^{-5}$  Gauss). At the geosynchronous orbit, the magnetic field strength is roughly  $1 \times 10^{-7} \text{ T}$  ( $100\gamma$ ). A magnetic field of this strength causes no threat per se to spacecraft operations; however, it plays a fundamental role in trapping energetic particles. These trapped particles respond not only to the Earth's magnetic field, but spacecraft fields as well, especially for spacecraft large in comparison to particle gyroradii (Reiff, 1976; Reiff and Burke, 1976).

Neutral particles have little effect on spacecraft operations above  $\sim 600$  km; however, neutrals can charge-exchange in the EOTV thruster beam (see below).

Charged particle populations at synchronous orbit are of several types and are illustrated in Figure 1. The innermost region is the plasmasphere, a torus-shaped locus of relatively dense ( $\sim 100/\text{cm}^3$ ), cool ( $kT \sim 1$  eV) plasma that has evaporated from the ionosphere. Because of the low energies of the plasmaspheric ions, they are considered harmless (Reasoner et al., 1976); however, they can be accelerated by spacecraft electric fields to energies high enough to do damage (tens of kilovolts). Imbedded in the plasmasphere are the radiation belts, regions of very low density but quite high energy (tens to hundreds of kilovolts) trapped radiation. This radiation can cause hazards to men and solar cells.

The remaining plasma population that can penetrate to geosynchronous orbit is the plasma sheet (Fig. 1). This tenuous plasma ( $0.1\text{-}1/\text{cm}^3$ ) is considerably warmer ( $kT$  on the order of kiloelectron volts) than the plasmasphere (Garrett and DeForest, 1979). In addition, its presence at geosynchronous orbit is associated with substorm activity, when both the fluxes and energies are higher. It is this kind of plasma that contributes most strongly to spacecraft charging and its concomitant disruption of satellite systems (Inouye, 1976).

This report concentrates on spacecraft charging and its effects on solar power satellite (SPS) systems, in particular the NASA/Marshall Space Flight Center (MSFC) baseline design (Hanley, 1978). "Worst case" plasma environments are used to determine possible charging hazards. Spacecraft charging is the principal focus of this paper since its effects can be severe: arc generation from exceeding breakdown voltages, direct electrical component damage from transients, disruption of logic and switching circuits from electromagnetic interference, change of reflective or thermal control surfaces due to the attraction of outgassed contaminants or pitting, and shock hazards for extravehicular and docking activities (see DeForest, 1972; Pike and Bunn, 1976; Shaw et al., 1976).

We will show that, under substorm conditions, the kapton substrate contemplated for use as a support blanket for the reflectors and solar cells will be subjected to near-breakdown voltage. Additional kapton insulation seems unfeasible because of weight considerations. The alternatives, higher conductivity substrates or conducting leads to the surfaces, seem more reasonable since the resulting parasitic currents are not excessive. The paper also will discuss the optimum point for grounding the spacecraft to the solar panels and outlines a method of using judicious routing of bus-bar currents to shield the satellite from particle bombardment. Although it is possible to use a similar method to magnetically align the satellite with the Earth's magnetic field (counteracting gravity-gradient torques), the fields required seem unreasonably large.

### Spacecraft Charging

A body immersed in a plasma will acquire a net charge from unequal fluxes of plasma particles. For most plasmas, the electron and ion densities  $N_e$  and  $N_i$  are roughly equal, and the electron and ion temperatures  $T_e$  and  $T_i$  are comparable. Thus the electron flux  $J_e$  (proportional to  $N_e \sqrt{kT_e/M_e}$ ) is generally much larger than the ion flux  $J_i$ , and the body acquires a negative charge sufficient to bring the currents into balance. For stationary, isothermal, singly-charged plasmas, the equilibrium unlit body potential is roughly  $(kT_e/e)\ln(J_e/aJ_i)$  (Whipple, 1965), where  $a$  is a parameter (of order unity) depending on the thickness of the sheath. Exposing the body to sunlight causes photoelectrons to be ejected. For most substances, the photoelectron current is on the order of one to four nanoamps per square centimeter. Since this is comparable to or larger than most space plasma electron currents, the surface will tend to acquire a small positive charge. The actual equilibrium potential will

depend on the details of the ion and electron distribution function, however (Whipple, 1976). The fluxes to a sunlit plate immersed in a plasma are shown schematically in Fig. 2. The lit side will tend to charge slightly positive, and the dark side negative.

The NASA MSFC baseline design (Hanley, 1978) is shown in Fig. 3. The surfaces on the satellite are divided into two types: active and passive, depending on whether or not voltages appear on the surface as a result of the satellite's own power supply. Passive surfaces include the solar reflectors and structural members. Active surfaces include the solar cells, interconnects, and bus bars. Active surfaces may attract or repel the ambient ions or electrons depending on the polarity of the surface voltage. Currents reach the passive surfaces only by photoemission and the thermal motion of ions and electrons. (We ignore backscattered and secondary electrons.)

### Calculation of Potentials

We make the simplifying assumption of a thin sheath (or 1-dimensional) approximation, i.e., the area collecting plasma is the actual geometrical area of the satellite (no focussing considered). The ambient electron and ion currents, therefore are, simply the thermal currents, given by

$$J_{i,e} = \frac{Ne}{4} \left( \frac{8kT}{\pi M} \right)^{1/2} \quad (1)$$

where  $N$ ,  $e$ ,  $T$ , and  $M$  are the number density, charge, temperature and mass for electrons or protons, depending on which current is calculated.

Parker (1979) has addressed the problem of a large flat-plate solar collector in space. He has found that the thin-sheath approximation is not valid at geosynchronous orbit for active structures. However, in the MSFC design, the passive, grounded reflecting panels form a trough in which the solar cells lie. Since the reflectors are conducting, they have a tendency to confine electric fields from the solar cells within the trough. This reduces the thick-sheath focussing effect because the electric fields do not penetrate significantly into space above the trough, and the reflectors themselves are barriers against plasma fluxes entering from the sides of the trough. Later in the paper we verify this assumption by showing results from a modified version of Parker's PANEL program for the special geometry of the MSFC design.

The analytic calculations below assume, for simplicity,

an intermediate sheath approximation; i.e., no focussing of outside plasma is considered, yet the sheath is large enough that photoelectrons from the reflectors can impact the solar cell, and vice versa.

For GEO, our assumed "worst case" plasma conditions are:  $N_e = N_i = 2/\text{cm}^3$ ,  $kT_e = 5 \text{ keV}$  and  $kT_i = 10 \text{ keV}$  (Inouye, 1976). This yields  $J_e = 3 \times 10^{-10} \text{ A/cm}^2$  and  $J_i = 1 \times 10^{-11} \text{ A/cm}^2$ .

The photoelectron current density was calculated by integrating the product of the photoelectron yield function for synthetic sapphire and the solar spectrum: the resulting photocurrent density  $J_{pe}$  is  $3 \times 10^{-9} \text{ A/cm}^2$ . A similar calculation for aluminum yields roughly the same photoelectron current density.

It is apparent, then, that the photoelectron current will usually dominate for all sunlit surfaces at GEO. The equilibrium potential for such surfaces will be on the order of a few times the average photoelectron energy, from about 1 to 100 V positive, such as is found on the dayside of the moon (Reasoner and Burke, 1972; Freeman and Ibrahim, 1975). Passive sunlit surfaces will attain this voltage; however, for active surfaces, the finite conductivity of the cover surfaces (kapton and sapphire) will prevent this voltage from being obtained, i.e., the surface potential will more nearly follow that of the underlying solar cell.

Nightside potentials are estimated from Chopra's (1961) equation:

$$\phi \approx - \frac{kT_e}{2e} \ln \left( \frac{M_i T_e}{M_e T_i} \right) \quad (2)$$

For the "worst case" described above, this implies a dark-side potential of -17,000 V. Secondary electron emission or backscattering will reduce this potential somewhat. Again, passive surfaces will attain this voltage, but most active surfaces will be more nearly the potential of the underlying solar cell.

The most vulnerable active surfaces on the satellite are the solar cells because the ohmic contacts are separated from the plasma by only tens of micrometers of shielding. Figure 4 shows the dimensions and structure of the solar cell selected in the MSFC design. The GaAlAs cell is supported from below by a kapton blanket and is covered with synthetic sapphire. The sapphire coverglass is 20  $\mu\text{m}$  thick and the kapton blanket is 25  $\mu\text{m}$  thick.

For our study, the solar cell was idealized as a sapphire - active region - kapton sandwich as shown in Fig. 5. Plasma ions were assumed to be attracted to the negatively biased portion of the solar array and plasma electrons to the positively biased portion. Photoelectrons were assumed to leave the negative surface and be attracted to the positive surface. Secondaries were neglected. The currents used were those described previously; we assume a steady state condition. In this case the voltages across the sapphire and kapton dielectrics are the photoelectron and plasma currents multiplied by the resistance of the dielectrics. The assumed resistivity of sapphire is  $10^{12}$  ohm-cm. Based on the measurements of Kennerud (1974) we have approximated the resistivity of kapton by

$$\rho = 9.2 \times 10^{16} \exp -[E/1.1 \text{ KV/mil}] \text{ ohm-cm,}$$

where E is the electric field across the kapton in KV/mil. The transcendental equation for the potential difference, V, through the 1-mil kapton layer is  $\ln [V/K] = -V/1100$ , where K is proportional to the current ( $K = 9 \times 10^{16} \times \text{thickness (cm)} \times \text{current (A/cm)}$ ). This equation was solved numerically. The resulting voltages are shown on Fig. 5: a drop of 949 V through the ion-attracting side, and a drop of 3.3 KV through the electron-attracting side. In no case are the breakdown voltages exceeded; however, the voltage on the positive array is within a factor of 2 of the breakdown voltage. For an electron current ten times larger (which can certainly occur within the satellite's life-span), the voltage drop is 5.4 kV, which is near breakdown. For this reason, we recommend replacing kapton with a higher conductivity material, or else providing a current path from the solar cell to the back side. Conductive coatings will also help reduce spot arcing (McCoy and Konradi, 1979).

Kennerud (1974) and others have found anomalous arcing when solar panels are held at high voltage negative in a plasma. Typical voltages and currents required for such anomalous arcing to take place are 400 volts at  $1 \times 10^{-7}$  A/cm<sup>2</sup>. Our expected ion currents to the negative portion of the solar array at GEO are  $1 \times 10^{-11}$  A/cm<sup>2</sup>. Therefore, we do not anticipate anomalous arcing in the GEO environment.

The MSFC design calls for the reflectors to be constructed from 0.5 mil (12.5  $\mu\text{m}$ ) kapton covered with a 400 A film of aluminum. We expect the aluminized front side potential to be fixed at 1 to 100 volts positive by photoelectron emission. Using the same analysis that was applied to the kapton solar cell blanket, we calculate the reflector back side voltage to be approximately -1.7 kV for our standard "worst case" condition, and -2.7 kV for a ten times

larger electron current. The breakdown voltage for 1/2 mil kapton is 3.1 kV, which could be reached with only slightly more severe plasma conditions. Clearly, the backside must also be conducting and electrically connected to the front, or the kapton must be replaced with a higher conductivity material. A summary of the expected voltages on various surfaces during sunlit and eclipse conditions is shown on Fig. 6. Note that during eclipse the entire satellite may charge to high voltage negative. This should be countered by the use of a hot filament electron emitter to bleed electrons from the spacecraft.

### Optimizing the Grounding Point

The currents between the satellite and the plasma will adjust until the net current is zero. This means that the flow of current to the positively biased areas must equal that from the negatively biased areas. In a flat plate collector, the balance is between plasma electron currents to the positive portions and plasma ion currents to the negative portions of the array. Since the plasma electron currents are so large, the plate will "float" substantially negative, i.e., the area of the collector with negative potential is much larger than the corresponding positive potential area (Parker, 1979).

In the MSFC design, however, the large aluminum reflectors are also sources and sinks of photoelectrons. Photoelectrons from the reflectors will be attracted to positive portions of the solar cell array and photoelectrons from the negative portions of the solar cell array will be attracted to the neighboring reflector (Figure 7). These electrons will "hop" along the surface (Pelizarri and Criswell, 1978), adding to the power drain. Thus the photoelectron current becomes the dominant parasitic current, at least in all but the most intense substorm environments.

The large aluminum reflectors make a convenient spacecraft ground, since the sunlit sides will remain a few volts positive with respect to space. To minimize the power drain, the solar cell array should drive no new currents through the reflectors to the plasma. Thus the reflector "ground" should be tied to the solar cells in an optimum way. Accurate calculation of the 3-dimensional electric field pattern and resultant power drain including effects of the space charge and secondaries is a formidable task; an oversimplified argument follows. If  $A^-$  is the solar cell area that is negative and  $A^+$  is the solar cell area that is positive, current balance requires

$$(A^-) (J_{pe} + 2J_i) = (A^+) (J_{pe} + 2J_e) \quad (3)$$

or, 
$$A^-/A^+ = (J_{pe} + 2J_e)/(J_{pe} + 2J_i).$$

Here we assume that the photoelectron flux from the reflectors to the positive segments is approximately the same as the photoelectron flux from the negative segments to the reflectors. For low plasma-current regions, (e.g., the plasmasphere or the quiet plasmashet) or for cases in which the plasma current is shielded from the surfaces magnetically, the ratio approaches unity. Even for our "worst case," the ratio is only 1.17. Therefore, we recommend grounding the midpoint of the string to the reflectors. On the other hand, at low Earth orbit plasma electron and ion ram fluxes dominate, and the grounding point must be more carefully calculated.

With the ground point determined, the parasitic load can be calculated. The principal parasitic current at GEO is from photoelectrons (Fig. 7), and is calculated to be about 3000 A. Coupled with an average potential drop of 11375 V, this implies a power loss of 34 MW, which is only 0.7% of output power, and is easily manageable by slight oversizing. This percentage power loss is comparable to that ( $\sim 0.1\%$ ) from a flat-plate collector (Parker, 1979). Thus optimizing the grounding point at GEO is not critical. As discussed later, however, at LEO optimization could be very important.

#### Currents at Low-Earth Orbit

An integral part of the SPS concept is the Earth-Orbit Transfer Vehicle (EOTV) which will transfer the SPS to GEO. It is expected to employ a high-voltage solar cell array and to operate primarily in the low-Earth orbit (LEO) environment where the plasma currents are considerably different than GEO. At 400 km altitude, the dominant ion is  $O^+$  with a number density of  $10^6/cm^3$  and a temperature of 2000 K (Johnson, 1965). Thus the thermal ion current will be  $7 \times 10^{-9}$  A/cm and the thermal electron current will be  $3 \times 10^{-7}$  A/cm. For these currents, the potentials on the EOTV will be comparable those for which Kennerud (1974) found arcing; therefore, one must expect arcing to take place on negatively-biased surfaces unless a lower-voltage array is used. Indeed, arcing has been observed from insulated surfaces in a LEO simulation vacuum tank test (McCoy and Konradi, 1979). Alternatively, the array could be biased with a minimum of negative surface (grounding the lowest end of the string to the reflectors), but that would be far from the optimum grounding scheme, and would increase parasitic losses by a factor of three.

Spacecraft motion implies a substantial though varying ram flux which will cause an additional parasitic current drain of as much as  $2 \times 10^{-7}$  A/cm<sup>2</sup>. Coupled with the cur-

rent losses due to the thermal currents, the power loss could be as high as ~3%. As noted, however, arcing probably will occur at much lower potentials than those for which 3% power loss would be observed. Parker (1979) has pointed out that sheath and wake effects also could substantially alter the satellite potentials and current flow.

### EOTV Parasitic Load Due to Thruster Charge-exchange Ions

An additional source of parasitic current for the EOTV is created by charge-exchange of ionized neutral gas from the thrusters with the energetic ions from the main thruster ion beam. This results in "thermal" ions which may drift into the Langmuir sheath electric field region surrounding the solar cell array. Once into the field they will be accelerated toward the solar cells and produce a parasitic load.

Following an approach outlined by H. R. Kaufman (NASA CR-135099) we have estimated the resulting parasitic load to the EOTV solar array to be 174 MW or 52% (Freeman and Few, 1979). This load is clearly unacceptable but it can easily be mitigated by placing a shield between the thrusters and the solar array. This shield can consist of an aluminized kapton sheet stretched across the end of the EOTV. The shield will need to have a height comparable to the dimensions of the Langmuir sheath, about 500 m. Additionally the low voltage edge of the solar cell array should be located toward the outside. Similar shields should be considered adjacent to the ACS thrusters on the SPS itself.

### Non-Steady State

Until now it has been assumed that the charging currents from the plasma are steady. This approach is supported by a study of the time dependent charging of a three-axis stabilized spacecraft by Massaro et al., (1977). For all the surfaces modeled, they found that the greatest differential voltages occurred in the steady state limit, although nearly instantaneous changes in absolute potential were observed. However, in order to evaluate the effects of non-steady charging, we calculated the RC time constant or discharge time of the relevant insulators, sapphire and kapton. The RC decay time is  $\rho\epsilon$  where  $\rho$  is the resistivity and  $\epsilon$  the permittivity. For kapton this implies a time constant of 1 hr; for sapphire, 1 sec. Large magnetospheric changes can occur with 1 min - 1 hr time constants (McIlwain, 1974; Inouye, 1976). Therefore, high voltages can build up on the kapton in time intervals short compared to the discharge time. Transient charging is not expected to cause differential charging in excess of the steady state predictions, nevertheless, the large kapton time constant reinforces the previous conclusion that kapton should be replaced with a higher conductivity material.

### 3-Dimensional Model

All of the foregoing analysis on parasitic loads, plasma induced voltages, etc., is based on one-dimensional plasma theory. More precise results require a three-dimensional self-consistent computer model which takes into account all plasma sources and interactions with reflectors simultaneously. A computer program, "PANEL" written by Dr. Lee Parker (Parker, 1979), provided a convenient starting point for our model of the SPS environment. Preliminary results will be presented here. They are preliminary since we have not yet included the photo-electron current (which we showed to be important), nor have we as yet included space charge effects. Nevertheless, the results demonstrate several important features of the sheath around the SPS troughs.

PANEL utilizes a three-dimensional grid where the satellite is modeled by fixing potentials at selected grid points. Laplace's equation is then satisfied by relaxing the free space potentials until Gauss's law is satisfied for a box surrounding each point. The currents and power losses are obtained by numerically performing the integral

$$J = \int_0^{\infty} dv \int_0^{\pi/2} d\theta \int_0^{2\pi} d\phi f(v, \theta, \phi) v^3 \cos\theta \sin\theta$$

where  $J$  is the current density, and  $f$  is the distribution function. The problem is then to evaluate  $f$ . For a collisionless steady state plasma, the Vlasov equation

$$\vec{v} \cdot \vec{\nabla} f + \frac{1}{m} \vec{F} \cdot \vec{\nabla}_v f = 0,$$

states that a distribution function

is constant along a particle's path in phase space. If  $f$  is written in terms of a particle's total energy ( $E = T + V$ , the kinetic plus potential energy),  $f$  will be constant in  $E$  along the path in real space. The integral for  $J$  is then transformed into a sum using the method of gaussian quadratures which picks key values of  $E$ ,  $\theta$ , and  $\phi$ . These values represent trajectories that are traced backwards to either source or nonsource regions to determine the value of  $f$ . Once the current is known it is multiplied by the local potential to determine the power loss at that point.

PANEL is a Laplacian calculation since space charge effects are not included in the electrostatic potential calculation. The next phase in the development of PANEL is to calculate the charge density for each point in space by evaluating the integral

$$N = \int_0^{\infty} dv \int_0^{\pi/2} d\theta \int_0^{2\pi} d\phi f(v, \theta, \phi) v^2 \sin\theta$$

in the same manner as described for the current calculation. Then PANEL must iterate between the potential relaxation routine and the density calculation since the density calculation depends upon the potential structure for accurate trajectories. This is known as the inside-out method (Parker, 1977) because trajectories are traced backwards in time.

Figure 8 illustrates the three dimensional grid used to model two interior panels of a trough. Not shown are grid points at the intersection of all integer  $x$  and  $y$  values and even values of  $z$ . One unit of grid spacing corresponds to 85.0 meters, giving model dimensions of 765 m X 425 m. Fixed voltages are indicated on the figure. The assumed plasma

conditions are  $N_i = N_e = 2/\text{cm}^3$ ,  $kT_i = 10 \text{ keV}$ ,  $kT_e = 5 \text{ keV}$ . For these conditions, the random thermal current densities are, as before:

$$J_{\text{th},i} = 1.25 \times 10^{-7} \text{ A/m}^2$$

$$J_{\text{th},e} = 3.79 \times 10^{-6} \text{ A/m}^2$$

The dimensionless numbers at selected points on the panels are ratios of local average electron current densities to the random electron thermal current. For the two panels modeled, PANEL traced 864 trajectories per grid square of surface. The resulting total current collected and power loss are  $6.64 \times 10^{-2} \text{ A}$ , and  $5.66 \times 10^2 \text{ W}$  for protons and  $2.25 \text{ A}$  and  $2.72 \times 10^4 \text{ W}$  for electrons. Calculated potential patterns in the  $x = 0$  plane and  $y = 3$  plane are shown in Figs. 9 and 10, respectively. Note that potentials of only 1-2 kV extend beyond the upper limits of the trough, justifying our earlier "intermediate sheath" approximation.

Photoelectrons from the reflectors and backscattered and secondary electrons undoubtedly will be important contributor to the power loss but have not yet been modeled.

#### Magnetic protection of the SPS

The SPS of necessity contains bus bars of current  $10^5 \text{ A}$ , routed between the solar panels and the microwave antennae. With judicious routing of these bus bars, the SPS can create its own protective magnetic barrier, screening out all the low energy ( $\sim 100 \text{ eV}$ ) plasmaspheric plasma (which can cause power drain), and most of the energetic electrons. Parker and Oran (1979) have shown that this idea is feasible with nominal bus-bar currents. We propose modified bus-bar currents to prevent spacecraft fields from merging with the earth's magnetic field. Merging can have two harmful effects:

- 1) It can channel energetic particles trapped in the Earth's magnetic field towards sensitive areas of the SPS.
- 2) It can energize the high density plasmaspheric plasma that would otherwise be harmless.

Previous spacecraft were small in size compared to particle gyroradii, so magnetic effects were not important. The size of the SPS, however, is comparable to particle gyroradii, so magnetic effects must be taken into account. (At geosynchronous orbit, a 2 eV proton or 3 keV electron has a gyroradius of 2 km; a 50 eV proton or 80 keV electron has a gyroradius of 10 km.) In the following, in order to estimate these effects (i.e., to repel trapped particles and to minimize energy released in magnetic merging) we assume

that it is important to have spacecraft magnetic fields parallel to sensitive areas (e.g., solar cells) and aligned with the Earth's magnetic field. (Even magnetic fields perpendicular to the surface can be beneficial, however, and have been considered in Parker and Oran, 1979).

A solenoidal bus-bar winding yields the best magnetic field configuration: at a distance, the field approaches that of a dipole, and in the vicinity of the satellite the field is parallel to the solar panels. The windings for the solenoid should enclose as much area as feasible. This will have two benefits: it will maximize the overall dipole moment while minimizing the bus bar length and thus IR losses, and will minimize the internal field. On the other hand, for spatial uniformity, one should have a least one turn per kilometer. Some possible cross-sections are shown in Fig. 11. This figure is a view from the north end of three types of trough-like SPS design and shows one turn of the helical winding each.

The field of the SPS must have sufficient rigidity to successfully deflect the species desired to be excluded. Table 1 show magnetic moments  $\mu$  required for various tasks. Two possible orientations of the SPS's dipole moment are compared: parallel or antiparallel to the Earth's dipole moment. A parallel orientation, since it adds to the local magnetic field, is more efficient at shielding the SPS from particle bombardment; however, the opposite orientation is dynamically more stable, since the SPS's moment will tend to align with the Earth's magnetic field. In fact, the moment may be used to balance gravity-gradient torques if the dipole moment is large enough. For a (uniform) body 22 km long and 4 km wide of mass  $5 \times 10^7$  kg, the moment of inertia about an axis perpendicular to the length of the satellite would be  $2 \times 10^{12}$  kg-m<sup>2</sup>. The daily  $\pm 10$  deg tilt of the geosynchronous magnetic field would cause a torque on the satellite of  $(\underline{\mu} \times \underline{B}) = 1.7 \times 10^4$  Nt-m, for a  $\mu = 10^{12}$  A-m<sup>2</sup> (corresponding to 0.9 Nt of force on each end). Since the satellite is so massive, this torque will result in a daily sinusoidal tilting motion of the satellite of amplitude  $\sim 10^{-5}$  degrees, completely negligible. A 10 deg tilt of the satellite toward the Earth, in contrast, will cause a gravity-gradient torque of  $2.7 \times 10^6$  Nt-m, or 125 Nt at each end, requiring a magnetic moment of  $1.5 \times 10^{14}$  A-m<sup>2</sup> to balance it. Then, however, the 10 deg misalignment between the spin axis and the dipole axis of the Earth would become more important. In addition, the magnetic fields in the SPS center would be quite large (90 G.). The internal field is sensitive to the exact configuration, and can vary by a factor of two or so depending on the area and number of turns per km. The rigidity, on the other hand, is not too sensi-

tive on the exact configuration, being mainly a function of overall magnetic moment.

One reasonable magnetic field configuration is shown in Figs. 12 - 14. The dipole moment assumed for these figures is the low-field case,  $10^{11}$  A-m<sup>2</sup> per km, 21 km total. All components of the field are, of course, linear in the dipole moment. This model superposes 21 dipoles at 1 km intervals (simulating one turn per km). Figure 12 shows vector magnetic fields for one quadrant; Fig. 13 shows contours of constant  $|B|$ , and Fig. 14 shows magnetic field components. Here the z-component is measured along the long axis and the  $\rho$  component is measured from the long axis. The center of the SPS is the lower left corner ( $z = 0$ ,  $\rho = 0$ ). Only one quadrant is shown because of symmetry:  $B_z(z) = B_z(-z)$ ;  $B_\rho(z) = -B_\rho(-z)$ . The field is similar to that of a solenoid and is nearly parallel to the long sides of the SPS (and therefore to the solar cells), converging at the SPS's north and south ends. (The SPS is aligned north-south to minimize the shadowing of one SPS on another in the equinox seasons.)

The field in Figs. 12 - 14 is strongest at the ends and weakest in the center; therefore, fewer wraps (or, more likely, less current per wrap) could be used at the ends and still obtain the same overall rigidity. A field of 100 extends to over 7 km from the center, and a field of 20 extends to 19 km. The overall rigidity at  $\rho = 1$  km,  $z = 0$  km is roughly  $2000\gamma$  - km (G-cm). With a magnetic field of this orientation and strength, ions  $< 200$  eV (including all the plasmaspheric plasma) and electrons  $< 30$  keV (most of the plasma sheet electron fluxes) are excluded. Higher dipole moments would yield more shielding (see Table 1). Thus, it appears that magnetic protection is feasible. Because of the convergence of the field, particle fluxes will have a tendency to strike only the ends of the long axis of the SPS. Simply capping the ends of the SPS, then, will be sufficient to protect electronics and humans inside from the lower-energy particles. Such capping is also useful to prevent the plasma from the ion engines from returning to the satellite, causing a significant power drain (Freeman and Few, 1979).

### Conclusions

The SPS will certainly interact with its plasma environment. It appears that, with relatively minor modifications to the NASA MSFC baseline design, these interactions will not significantly impair SPS operations. The conclusions and recommendations of this study include:

- 1) Arcing is likely to occur on kapton surfaces (the solar reflectors and the solar cell back surface blanket)

during substorms unless the kapton is replaced by a lower resistivity material ( $\rho < 10^{13}$  ohm-cm) or current paths from the surfaces to the solar cells are provided.

2) The SPS parasitic load under normal conditions will be about 34 MW (for a 5 GW array) at geosynchronous orbit. This 0.7% power loss should be accommodated by oversizing.

3) The optimum grounding point at GEO for the SPS solar cell array is approximately the midpoint on the voltage string. At LEO, arcing considerations demand that the string be biased mostly positive, although the optimum configuration to minimize power loss would be substantially negative (see conclusion 5).

4) The solar cells may require conductive coatings. The reflector panels may require current paths linking the front and back sides. Laboratory tests in a substorm simulator on realistic solar panels are recommended to determine the actual arcing probability.

5) Severe arcing problems are expected for negative portions of the EOTV solar cell array at LEO. Overcoming this problem by biasing the array as positive as possible will result in high parasitic loads (power losses on the order of 3%). Only a low voltage EOTV solar array should be used.

6) The SPS will occasionally charge to about -20 kV during eclipses. An active discharge method such as a hot filament electron emitter should be provided.

7) A shield should be placed across the ends of the EOTV to prevent thruster ion feedback to the solar array. Similar shields may be required on the SPS.

8) Three-dimensional computer modeling of the SPS electric field pattern and plasma currents is underway. The model shows that, for the grounding scheme used here, spacecraft electric fields extend only slightly beyond the reflectors.

9) Active magnetic plasma shielding is possible through judicious routing of bus-bars; power drain from additional lengths of bus-bars has not been calculated yet.

10) It is possible to use the internal magnetic field to align the satellite (counteracting gravity-gradient torques), but it would require an unreasonably large magnetic moment ( $1.5 \times 10^{14}$  A-m<sup>2</sup>).

#### Acknowledgments

The authors thank Dr. Lee Parker for consultation and the use of the computer program "PANEL." In addition, we have benefited from discussion with Dr. James McCoy. This work was supported by NASA under grant NAS8-33023.

The computer program PANEL is attached as appendix A.

## References

- Burke, W. J., Reiff, P. H., and Reasoner, D. L., "The Effect of Local Magnetic Fields on the Lunar Photoelectron Layer While the Moon Is in the Plasma Sheet," Geochemica Cosmochemica Acta, Suppl. 6, Vol. 3, 1975, pp. 2985-2997.
- Chopra, K. P., Reviews of Modern Physics, Vol. 33, 1961, p. 153.
- DeForest, S. E., "Spacecraft Charging at Synchronous Orbit," Journal of Geophysical Research, Vol. 77, February, 1972, pp. 651-659.
- Freeman, J. W. and Few, A. A., "Electrostatic Protection of the Solar Power Satellite And Rectenna," final report, NASA contract NAS8-33023, Rice University, Houston, Texas, May 1979.
- Freeman, J. W. and Ibrahim, M., "Lunar Electric Fields, Surface Potential And Associated Plasma Sheets," The Moon, Vol. 14, 1975, pp. 103-114.
- Garrett, H. B. and DeForest S. E., "Analytic Simulation of the Geosynchronous Plasma Environment," Planetary Space Science, Vol 26, (in press), 1979.
- Hanley, G. M., "Satellite Power Systems (SPS) Concept Definition Study," final report for NASA contract NAS8-32475, Rockwell International Report #5078-AP-0023, Cincinnati, 1978.
- Inouye, G. T., "Spacecraft Potentials in A Substorm Environment," Progress in Astronautics and Aeronautics: Spacecraft Charging by Magnetospheric Plasmas, ed. by A. Rosen, AIAA, New York, 1976, pp. 103-120.
- Johnson, F. S (ed). Satellite Environment Handbook, Stanford University Press, Stanford, California, 1965.
- Kennerud, K. L., "Final Report High Voltage Solar Array Experiments," Boeing Aerospace Corp., Seattle, Wash., Rept. No. CR121280, 1974.
- Massaro, M. J., Green, T., and Ling, P., "A Charging Model for Three-axis Stabilized Spacecraft," Proceedings of the Spacecraft Charging Technology Conference, edited by C. P. Pike and R. R. Lovell, Air Force Rept. AFGL-TR-77-0651, 1977, pp. 237-267.

McCoy, J. E. and Konradi, A., "Sheath Effects Observed on A 10 Meter High Voltage Panel in Simulated Low Earth Orbit Plasma," Space Craft Charging Technology-1978, edited by R. C. Finke and C. P. Pike, NASACP 2071, 1979, pp. 315-340.

McIlwain, C. E., "Substorm Injection Boundaries," Magnetospheric Physics, edited by B. M. McCormac, D. Reidel, Hingham, Mass., 1974, p. 143.

Mizera, P. F. and Fennell, J. F., "Satellite Observations of Polar, Magnetotail Lobe, and Interplanetary Electrons at Low Energies," SAMSO Rept TR-78-6, 1978.

Parker, L. W., "Plasma Sheath Effects and Voltage Distributions of Large High-power Satellite Solar Arrays," Spacecraft Charging Technology-1978, edited by R. C. Finke and C. P. Pike, NASA CP 2071, 1979, pp. 341-357.

Parker, L. W. and Oran, W. A., "Magnetic Shielding of Large High-power-satellite Solar Arrays Using Internal Currents," Spacecraft Charging Technology-1978, edited by R. C. Finke and C. P. Pike, NASA CP 2071, 1979, pp. 376-387.

Parker, L. W., "Calculation of Sheath and Wake Structure about A Pillbox-shaped Spacecraft in A Flowing Plasma," Proceedings of the Spacecraft Charging Technology Conference, edited by C. P. Pike and R. R. Lovell, Air Force Report AF6L-TR-77-0051, 1977, pp. 331-336.

Pelizzari, M. A. and Criswell, D. R., "Differential Photoelectric Charging of Nonconducting Surfaces in Space," Journal of Geophysical Research, Vol. 83, November, 1978, pp. 5233-5244.

Pike, C. P. and Brun, M. H., "A Correlation Study Relating Spacecraft Anomalies to Environmental Data," Progress in Astronautics and Aeronautics: Spacecraft Charging by Magnetospheric Plasmas, edited by A. Rosen, AIAA (New York), 1976, pp. 45-60.

Reasoner, D. L. and Burke, W. J., "Characteristics of the Lunar Photoelectron Layer," Journal of Geophysical Research, Vol. 77, December, 1972, pp. 6671.

Reasoner, D. L., Lennartsson, W., and Chappell, C. R., "Relationship Between ATS-6 Spacecraft-charging Occurences and Warm Plasma Encounters," Progress in Astronautics and Aeronautics: Sapcecraft Charging by Magnetospheric Plasmas, edited by A. Rosen, AIAA, New York, 1976, pp. 89-101.

Reiff, P. H., "Magnetic Shadowing of Charged Particles by An Extended Surface," Journal of Geophysical Research, Vol. 81, July, 1976, pp. 3423-3427.

Reiff, P. H. and Burke, W. J., "Interactions of the Plasma Sheet with the Lunar Surface at the Apollo 14 Site," Journal of Geophysical Research, Vol 81, September, 1976, pp. 4761-4764.

Shaw, R. R., Nanevicz, J. W., and Adamo, R. C., "Observations of Electrical Discharges Caused by Differential Charging," Progress in Astronautics and Aeronautics: Spacecraft Charging by Magnetospheric Plasmas, edited by A. Rosen, AIAA, New York, 1976, pp. 61-79.

Whipple, E. C., Jr., "The Equilibrium Electric Potential at A Body in the Upper Atmosphere and in Interplanetary Space," NASA T. N. X-615-65-296, 1965.

Whipple, E. C., Jr., "Theory of the Spherically Symmetric Photoelectron Sheath: A Thick Sheath Approximation and Comparison with ATS6 Observation of a Potential Barrier," Journal of Geophysical Research, Vol. 81, February, 1976, pp. 601-607.

## FIGURE CAPTIONS

Fig. 1 Sketch of the Earth's magnetosphere (from Mizera and Fennell, 1978).

Fig. 2 Schematic of plasma and photoelectron currents.

Fig. 3 Sketch of the MSFC January 25, 1978, baseline design (from Hanley, 1978).

Fig. 4 Cross-section of a proposed GaAlAs solar cell (from Hanley, 1978).

Fig. 5 Idealization of the solar cell blanket, used in calculations of electrostatic potential, for the "worst case" plasma fluxes.

Fig. 6 Summary of voltages on the reflectors and solar cells surfaces, for solar cells at large positive voltages (top), large negative voltages (middle), and during eclipse (bottom). (Midpoint of the solar cell voltage string is assumed to be grounded to the sunlit side of the reflectors.)

Fig. 7 Summary of parasitic current densities for the SPS and the parasitic current and power loss total for one half of the Marshall satellite (5 GW system).

Fig. 8 Computer grid used to model 2 panels of the SPS. (Small numbers on the panel surface are the plasma electron currents normalized to random thermal currents.)

Fig. 9 Equipotential contours in the yz plane at  $x = 0$  (indicated in Fig. 8).

Fig. 10 Equipotential contours in the xz plane at  $y = 3$  (indicated in Fig. 8).

Fig. 11 Recommended current windings for several SPS configurations (view from north end).

Fig. 12 Vector magnetic fields for a solenoidal current configuration, low-field case ( $\mu = 10^{11}$  A-m<sup>2</sup> per km, 21 km total). (Z-axis is along the spacecraft ( $z = 0$  is the center), and  $\rho$  is measured from the spacecraft axis; only one quadrant is shown, because of symmetry:  $B_z(-z) = B_z(z)$ ;  $B_\rho(-z) = -B_\rho(z)$ .)

Fig. 13 Contours of constant  
 $|B|$  for the low-field case.  
Only one quadrant is shown.

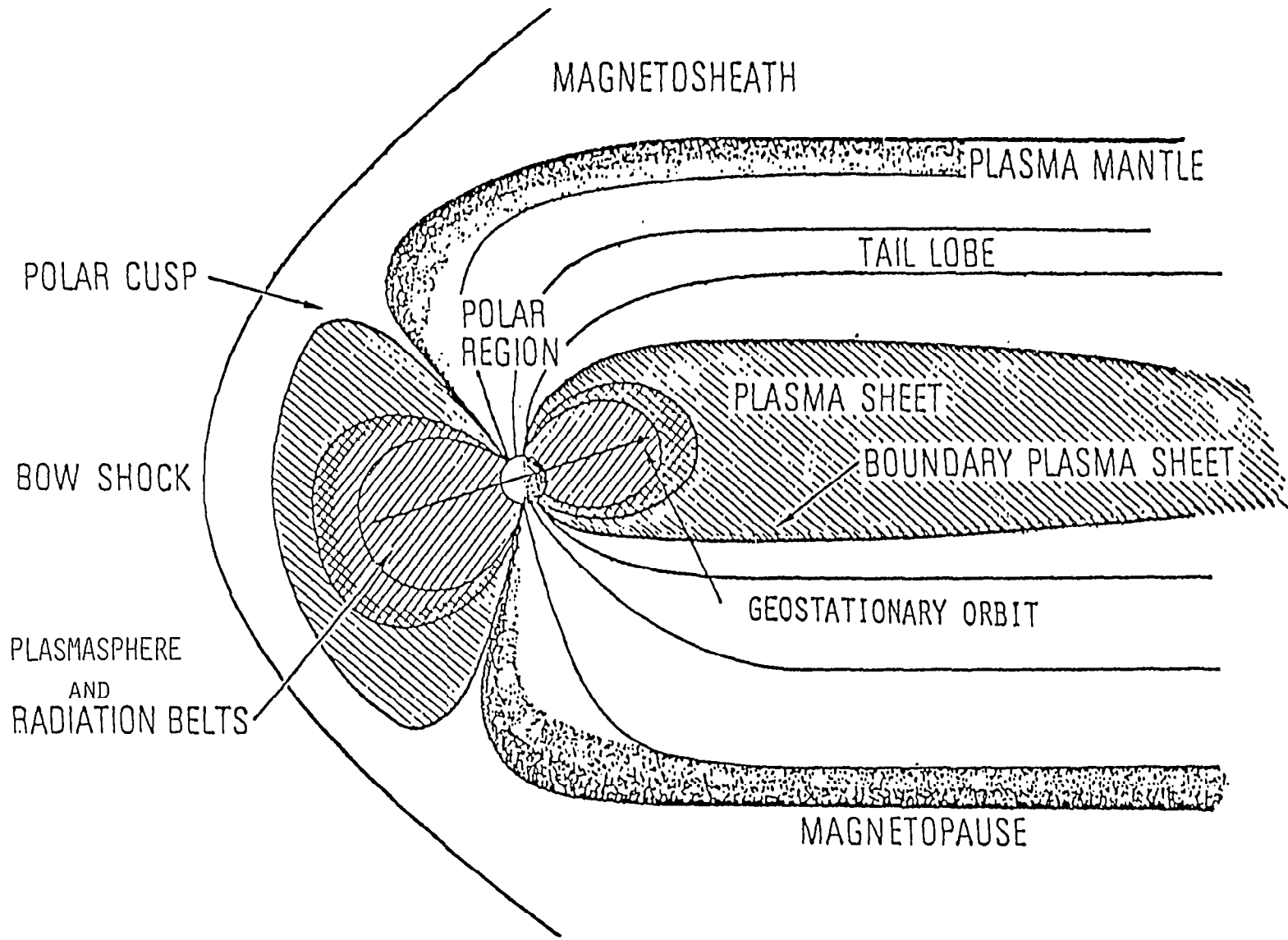
Fig. 14 Contours of constant  $B_\rho$  and  $B_z$ , low-field case.

### Magnetic Moment Required for SPS Tasks

Task	Rigidity Required	Orientation Of Moment	Internal Field (Gauss)	Required Moment- $A\text{-m}^2/\text{km}^\dagger$
Shielding 200 eV Protons and 30 keV Electrons	$2 \times 10^3$	*Parallel	1.3	$1 \times 10^{11}$
		*Antiparallel	4	$3 \times 10^{11}$
Shielding 3 KeV Protons and 2 MeV Electrons	$8 \times 10^3$	*Parallel	5.3	$4 \times 10^{11}$
		*Antiparallel	11	$8 \times 10^{11}$
Shielding 30 KeV Protons 10 MeV Electrons	$3 \times 10^4$	Parallel	20	$1.5 \times 10^{12}$
		*Antiparallel	25	$2 \times 10^{12}$
Magnetic Alignment (Balance Gravity- Gradient)	N/A	*Antiparallel	92	$7 \times 10^{12}$

\*Recommended Orientation

†Multiply by 21 for total magnetic moment.



20

Figure 1

A BODY IN A PLASMA PLUS SUNLIGHT

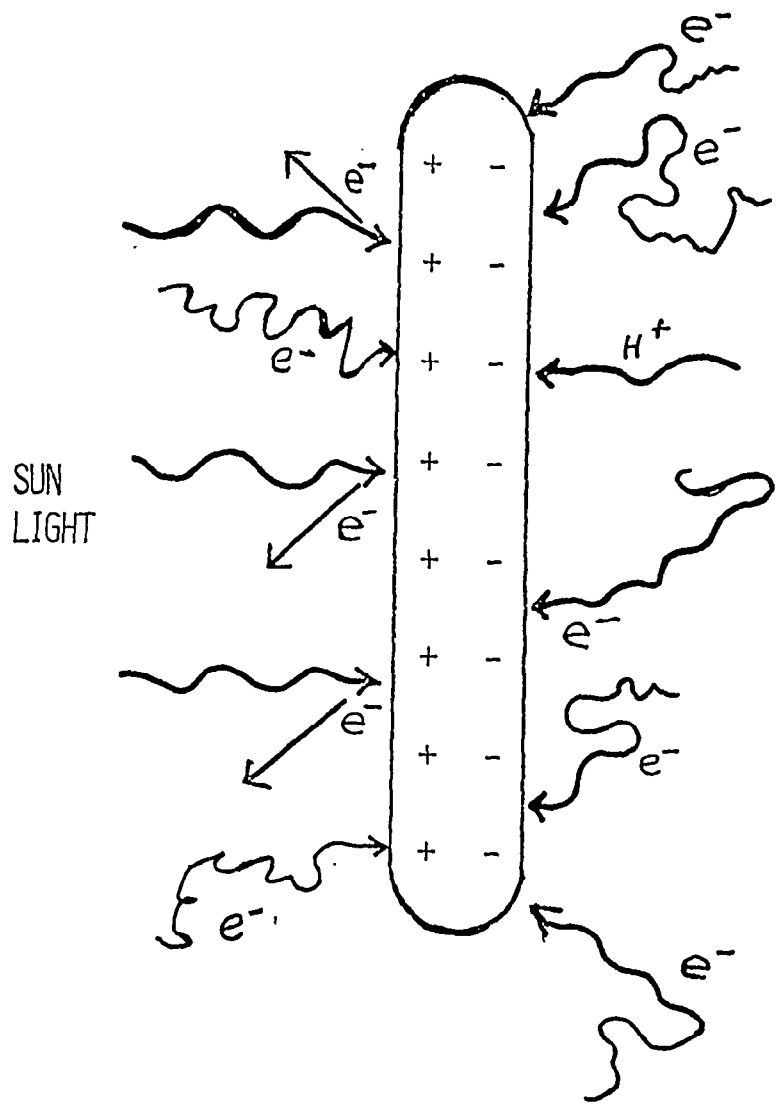


Figure 2

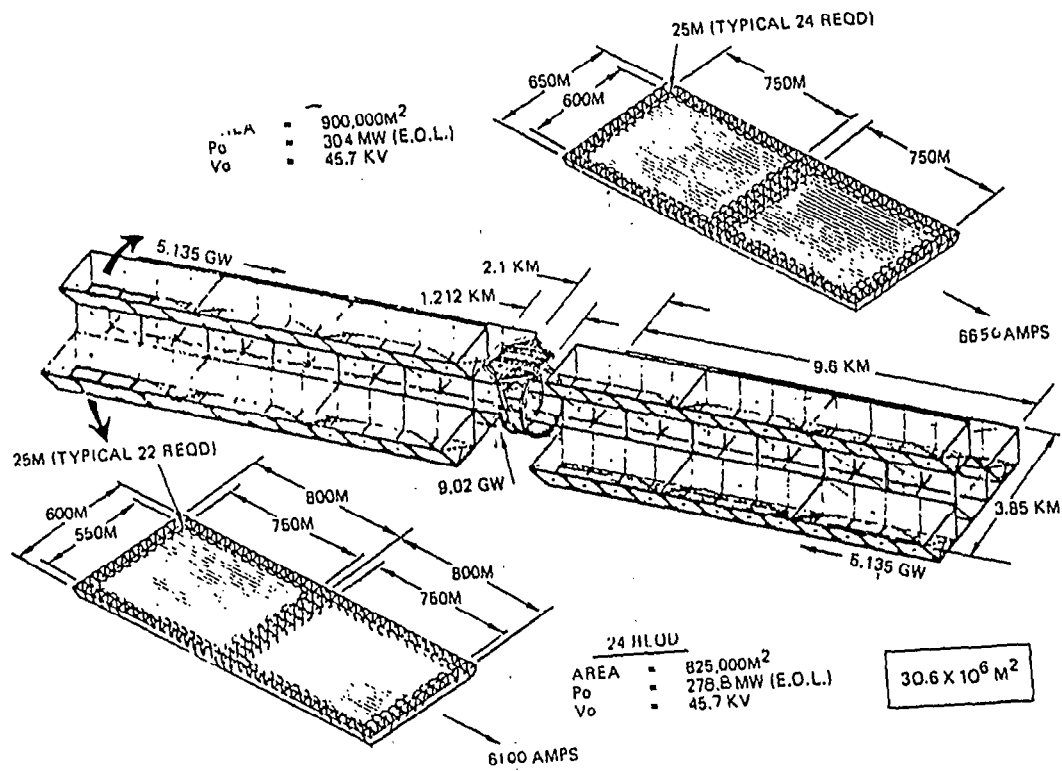


Figure 3

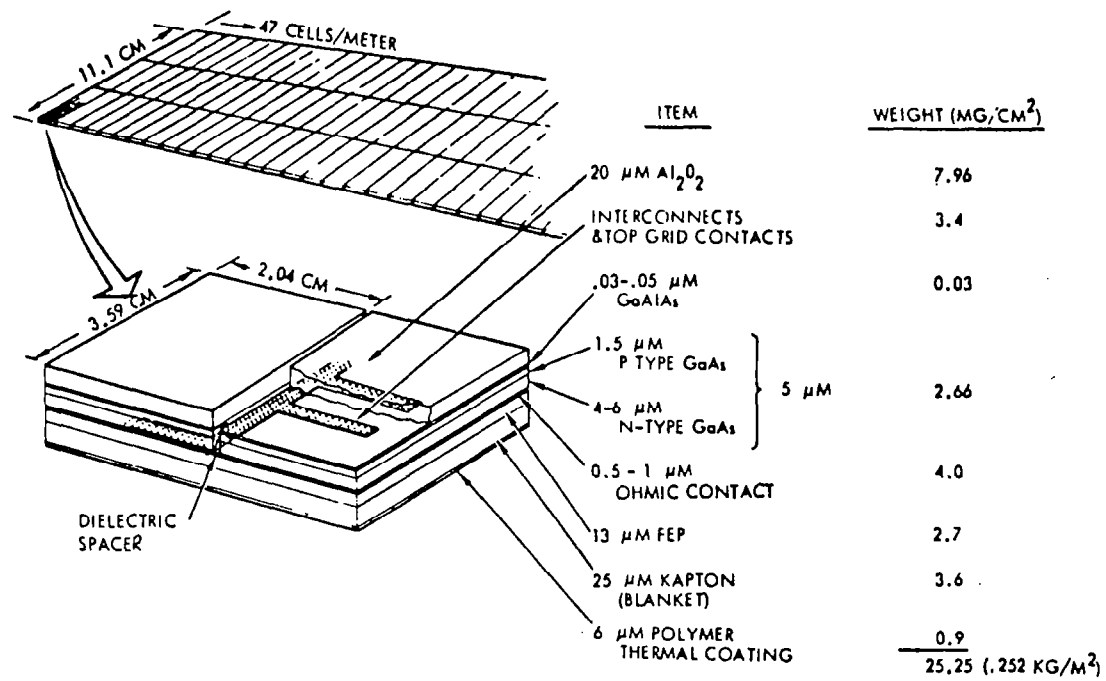
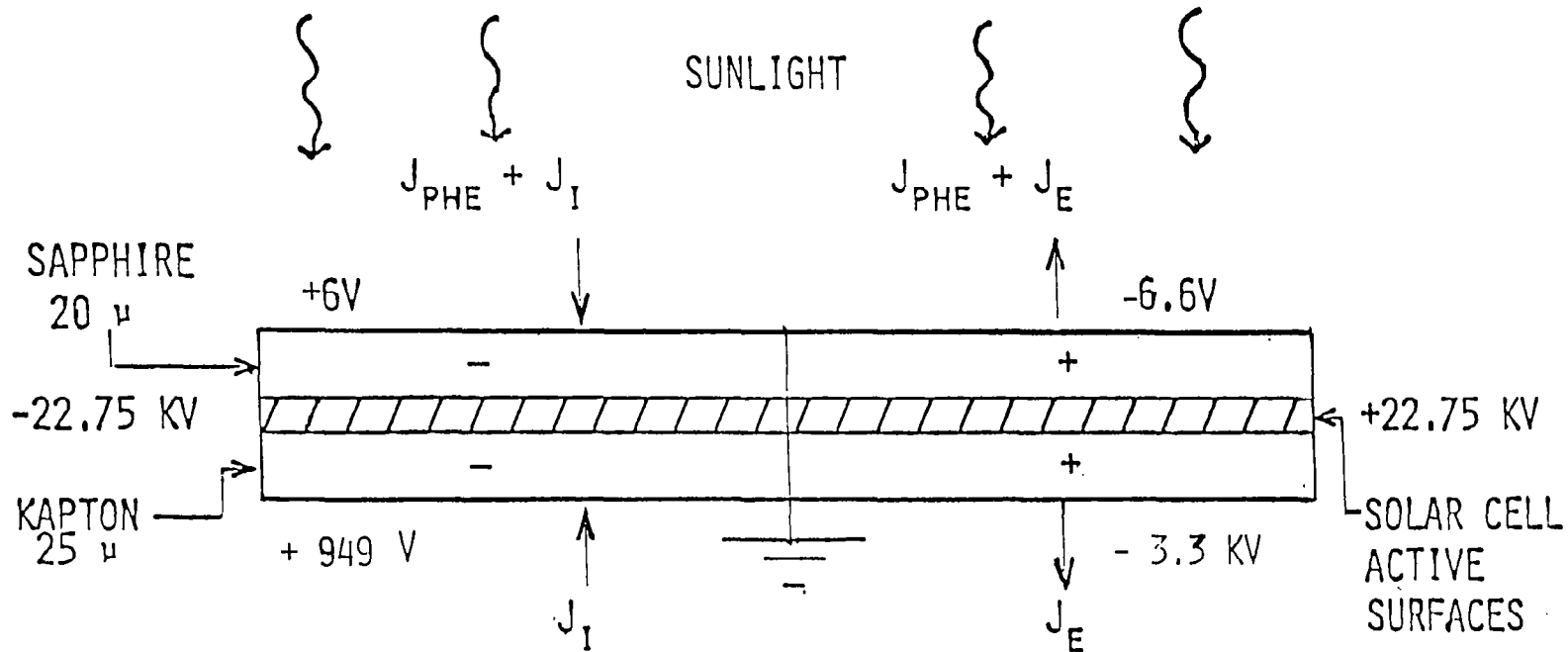


Figure 4

ACTIVE SURFACES (SOLAR CELL BLANKET):



24

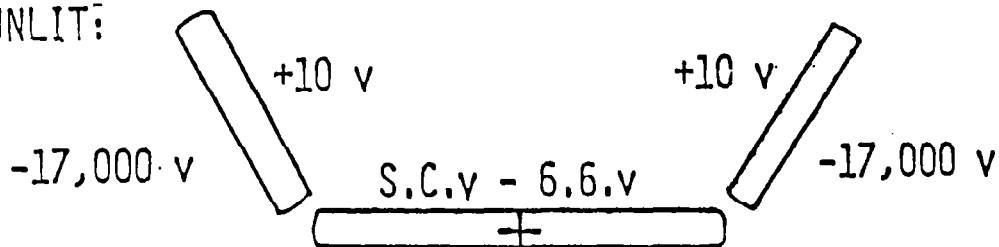
VOLTAGES SHOWN ARE RELATIVE TO THE LOCAL SOLAR CELL VOLTAGE. THEY REPRESENT THE IR DROP ACROSS THE COVER GLASS OR KAPTON BLANKET.

\* THE KAPTON BREAKDOWN VOLTAGE IS ~ 6250 V

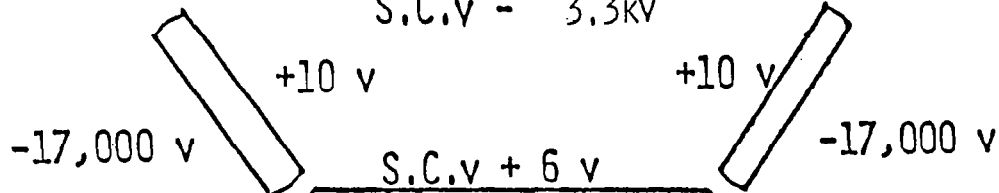
Figure 5

SUMMARY OF VOLTAGES:

SUNLIT:



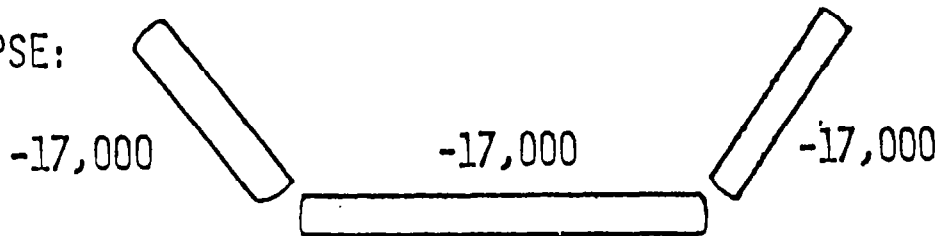
S.C.v - 3.3kv



S.C.v + 949 v

INDICATES SOLAR CELL ARRAY POLARITY

ECLIPSE:



-17,000

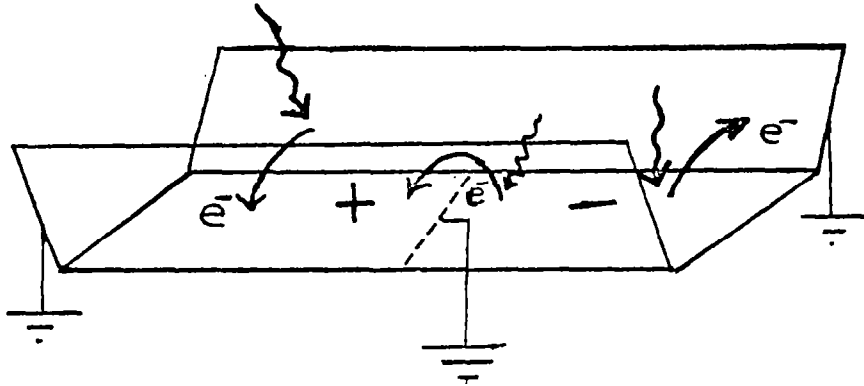
Figure 6

THE VARIOUS CURRENT DENSITIES ARE:

$$J_{\text{PHE}} = 3 \times 10^{-9} \text{ AMP/CM}^2 \text{ (FOR SAPPHIRE)}$$

$$J_{\text{E (PLASMA)}} = 3 \times 10^{-10} \text{ AMP/CM}^2$$

$$J_{\text{I (PLASMA)}} = 1 \times 10^{-11} \text{ AMP/CM}^2$$



PHOTOELECTRON FLOW DIRECTIONS

TOTAL PARASITIC CURRENT:

$$I_{\text{P}} \approx 3000 \text{ AMPS}$$

$$\bar{V} = 11,375 \text{ V}$$

THE PARASITIC POWER IS:

$$P_{\text{P}} \approx 34 \text{ MW}$$

(0.7% OF OUTPUT POWER)

Figure 7

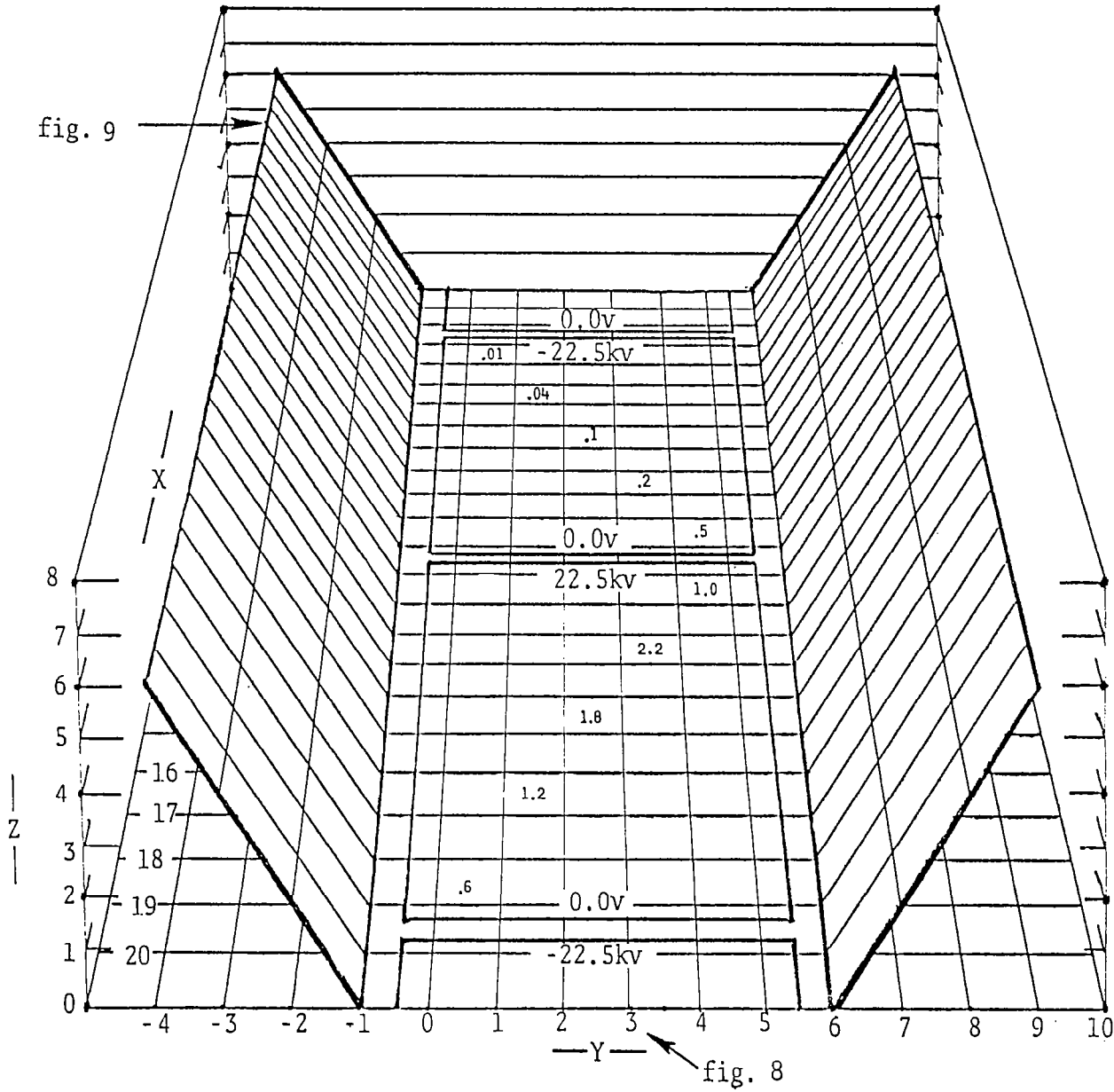
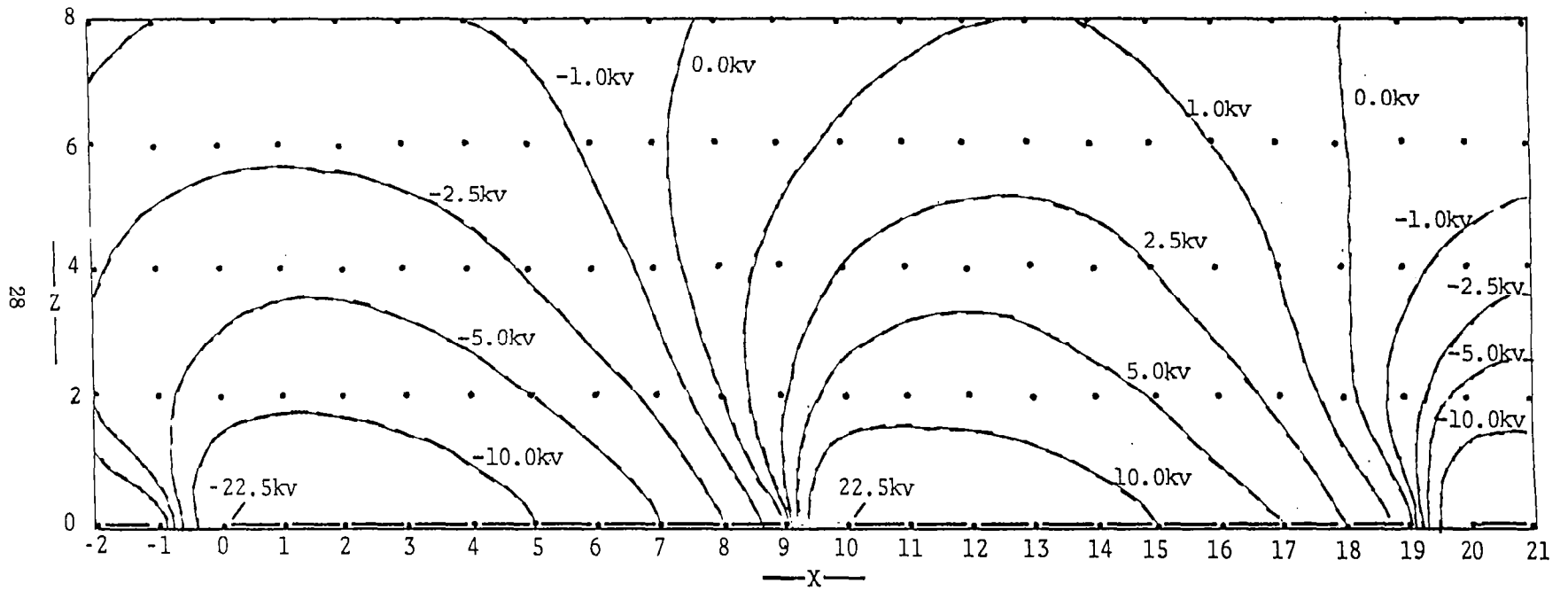
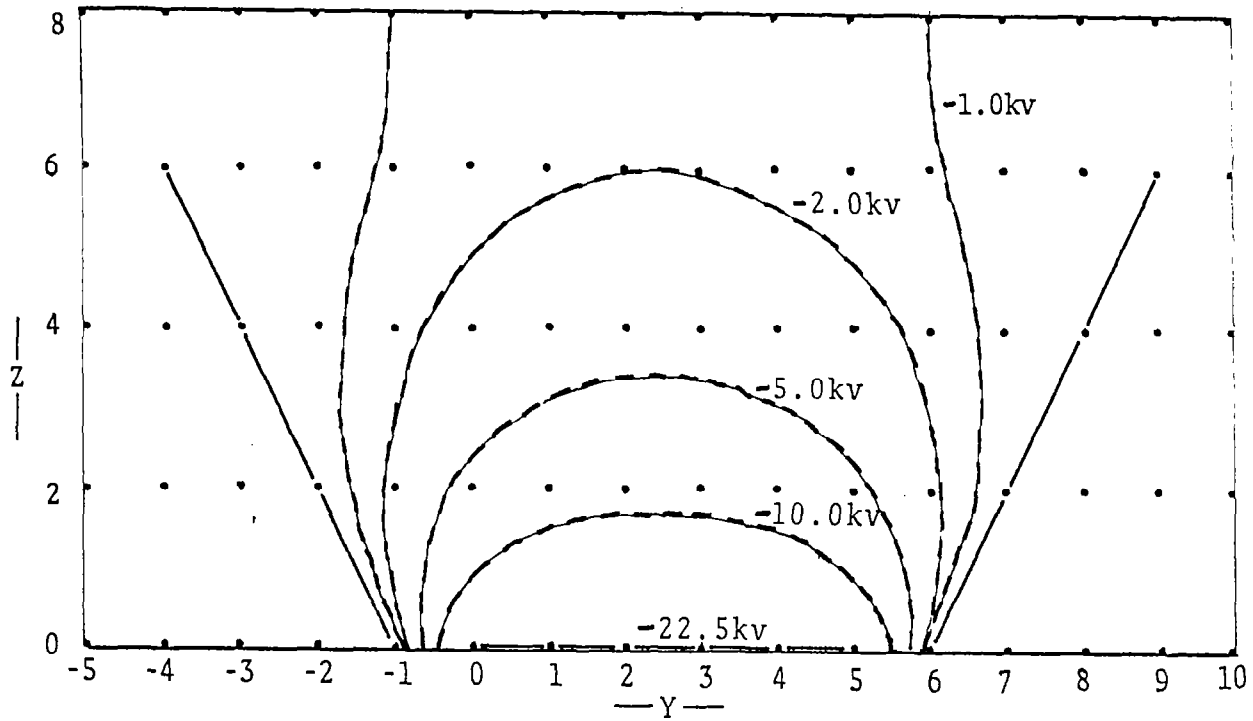


Figure 8



EQUIPOTENTIALS IN THE Y=3 PLANE

Figure 9

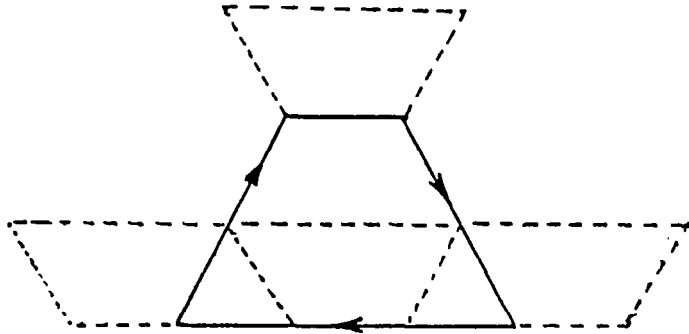


EQUIPOTENTIALS IN THE  $X=0$  PLANE

Figure 10

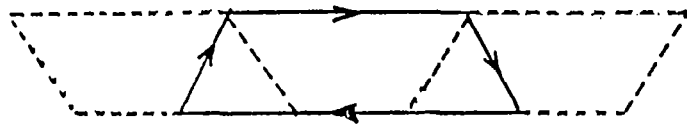
RECOMMENDED BUS BAR CURRENT CONFIGURATIONS

PREFERRED CONFIGURATION



AREA =  $1,6 \times 10^6 \text{ M}^2$   
LOOP LENGTH = 5200 M  
1-4 TURNS PER KM RECOMMENDED

30

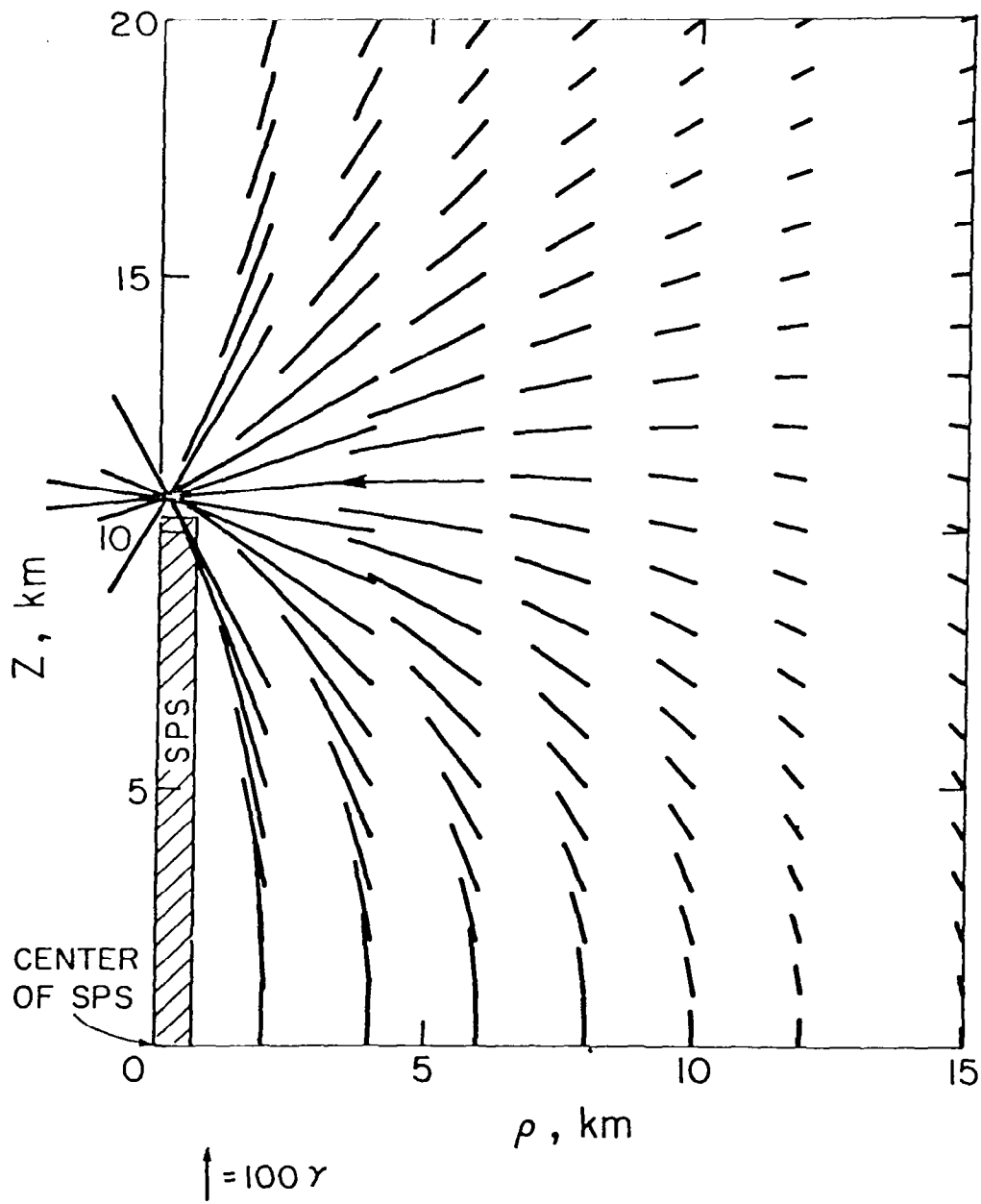


AREA =  $9,1 \times 10^5 \text{ M}^2$   
LOOP LENGTH = 4300 M  
1-6 TURNS PER KM RECOMMENDED



AREA =  $2,4 \times 10^6 \text{ M}^2$   
LOOP LENGTH = 9500 M  
1-2,5 TURNS PER KM RECOMMENDED

Figure 11



VECTOR MAGNETIC FIELDS

Figure 12

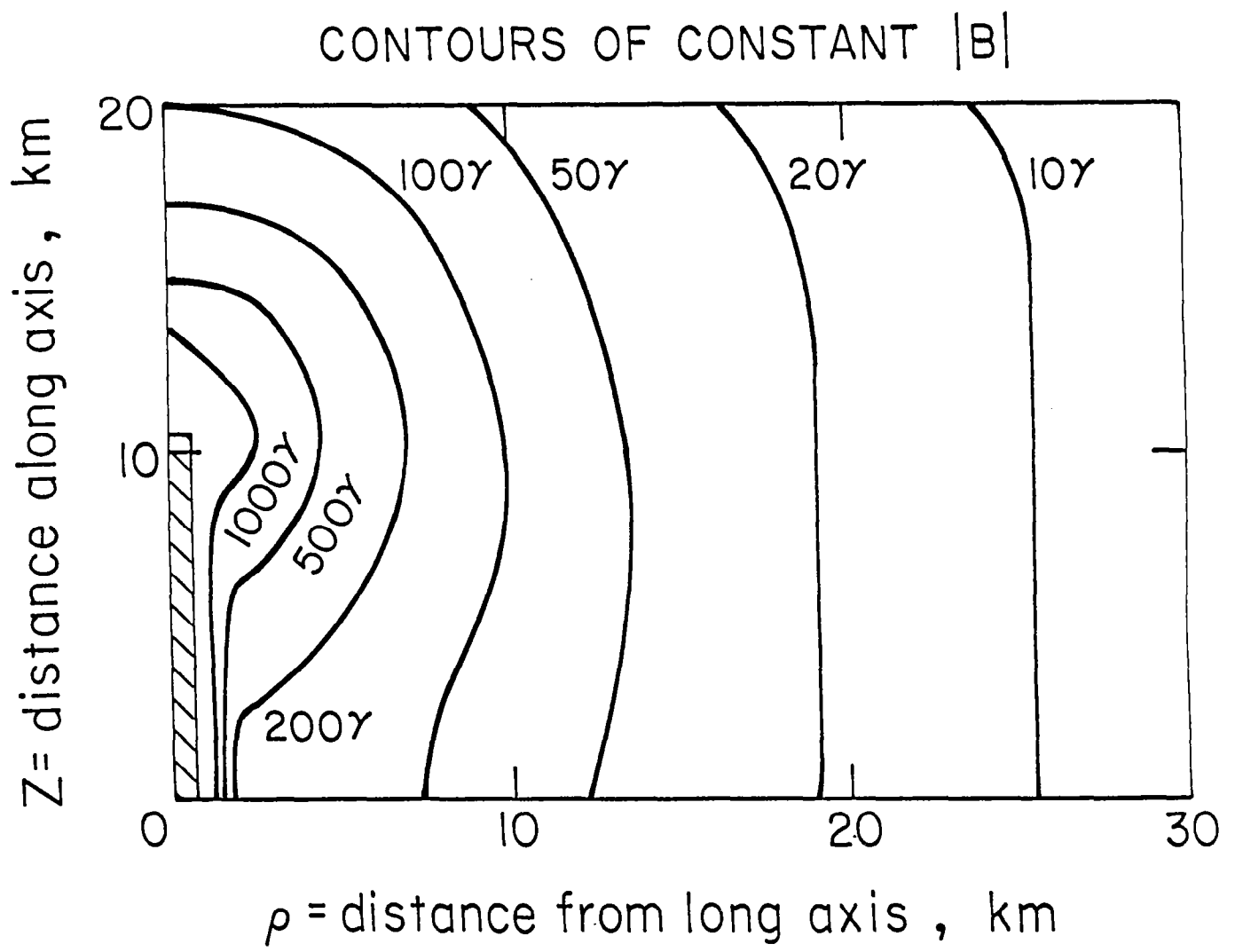


Figure 13

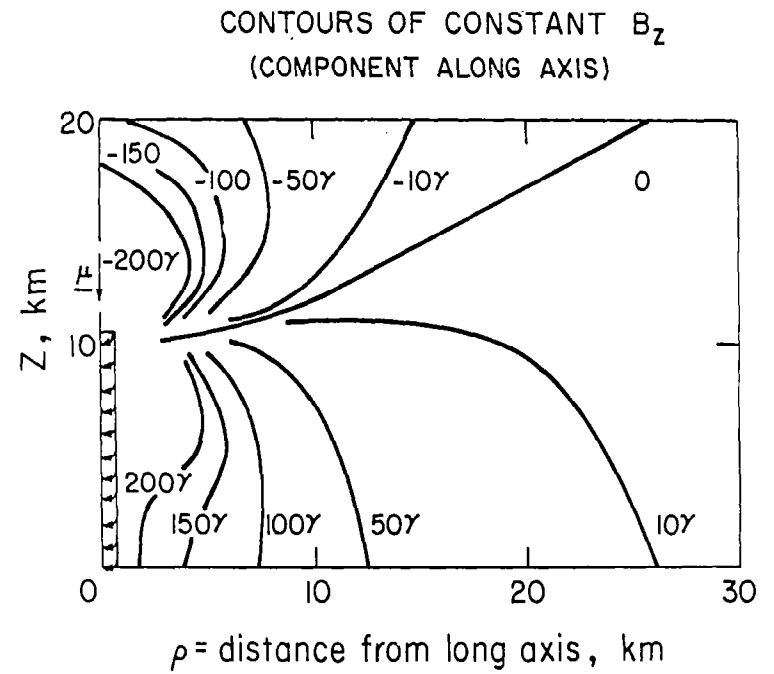
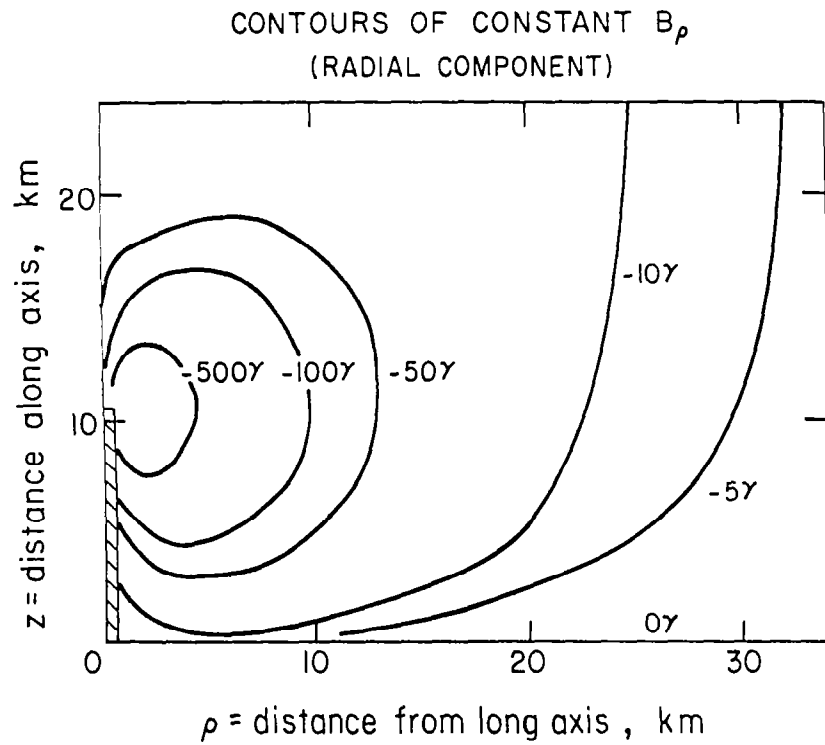


Figure 14

1. REPORT NO. NASA CR-3344	2. GOVERNMENT ACCESSION NO.	3. RECIPIENT'S CATALOG NO.	
4. TITLE AND SUBTITLE Electrostatic Protection of the Solar Power Satellite and Rectenna Part I: Protection of the Solar Power Satellite		5. REPORT DATE November 1980	
		6. PERFORMING ORGANIZATION CODE	
7. AUTHOR(S)		8. PERFORMING ORGANIZATION REPORT #	
9. PERFORMING ORGANIZATION NAME AND ADDRESS Rice University Houston, Texas 77001		10. WORK UNIT NO. M-308	
		11. CONTRACT OR GRANT NO. NAS8-33023	
12. SPONSORING AGENCY NAME AND ADDRESS National Aeronautics and Space Administration Washington, DC 20546		13. TYPE OF REPORT & PERIOD COVERED Contractor Report	
		14. SPONSORING AGENCY CODE	
15. SUPPLEMENTARY NOTES NASA Marshall Technical Monitor: Charles Guttman Final Report			
16. ABSTRACT  This report examines theoretically several features of the interactions of the Solar Power Satellite (SPS) with its space environment. We calculate the voltages produced at various surfaces due to space plasmas and the plasma leakage currents through the kapton and sapphire solar cell blankets. At geosynchronous orbit (GEO), this parasitic power loss is only 0.7%, and is easily compensated by oversizing. At low-earth orbit, (LEO), the power loss is potentially much larger (3%), and anomalous arcing is expected for the EOTV high voltage negative surfaces. Preliminary results of a three-dimensional self-consistent plasma and electric field computer program are presented, confirming the validity of the predictions made from the one-dimensional models. Lastly, the report considers magnetic shielding of the satellite, to reduce the power drain and to protect the solar cells from energetic electron and plasma ion bombardment. We conclude that minor modifications can allow the SPS to operate safely and efficiently in its space environment. The SPS design employed in this study is the Jan 25, 1978 MSFC baseline design utilizing GaAs solar cells at CR-2 and an aluminum structure. Subsequent design changes will substantially alter the basic conclusions in this report.			
17. KEY WORDS Magnetic field Charged particles		18. DISTRIBUTION STATEMENT Unclassified - Unlimited  Subject Category 44	
19. SECURITY CLASSIF. (of this report) Unclassified	20. SECURITY CLASSIF. (of this page) Unclassified	21. NO. OF PAGES 34	22. PRICE A03

For sale by National Technical Information Service, Springfield, Virginia 22151